Received: 15 May 2023 | Revised: 20 September 2023 | Accepted: 2 November 2023

DOI: 10.1002/zamm.202300390

ORIGINAL PAPER

Inverse multiquadric kernel-based neuro heuristic approach to analyze the unsteady MHD nanofluid flow via permeable elongating surface

Zeeshan Ikram Butt[1] | **Iftikhar Ahmad**[1] | **Syed Ibrar Hussain**[2] | **Muhammad Asif Zahoor Raja**[3] | **Muhammad Shoaib**[4] | **Hira Ilyas**[1]

[1]Department of Mathematics, University of Gujrat, Gujrat, Pakistan

[2]Dipartimento di Matematica e Informatica, Università degli Studi di Palermo, Palermo, Italy

[3]Future Technology Research Centre, National Yunlin University of Science and Technology, Douliou, Yunlin, Taiwan, R.O.C.

[4]AI Center, Yuan Ze University, Taoyuan, Taiwan

Correspondence
Syed Ibrar Hussain, Dipartimento di Matematica e Informatica, Università degli Studi di Palermo, Via Archirafi 34, 90123, Palermo, Italy.
Email: syedibrar.hussain@unipa.it

Muhammad Asif Zahoor Raja, Future Technology Research Centre, National Yunlin University of Science and Technology, 123 University Road, Section 3, Douliou, Yunlin, 64002, Taiwan.
Email: rajamaz@yuntech.edu.tw

In this study, a novel neuro heuristic approach is designed to investigate the flow properties of magnetohydrodynamic (MHD) nanofluid along an exponentially extending sheet with a permeable medium with the impact of radiation as well as fluctuating heat source/sink. The designed scheme to handle the suggested problem is established through the well-known biologically inspired neural networks (BINNs) by exploiting the inverse multiquadric kernel (IMQK), that is, BINNs-IMQK which is quite a new approach. The partial differential equations (PDEs) which govern the fluidic flow are reformed into a nonlinear system of ordinary differential equations (ODEs) using the most fitted similarity transformations rules and numerically solved by varying the parametric values including unsteady parameter, Brownian motion parameter, suction/injection parameter, radiation parameter, Schmidt number together with Prandtl number to visualize the velocity, thermal gradient, and mass transfer in the suggested fluid problem. It is noticed that nanofluid temperature hikes by uplifting the value of the Brownian motion parameter but this effect is reversed in case of unsteady parameter. The obtained numerical results are verified through reference solution using the well-known Adams method and the efficacy of the suggested solver is endorsed using a variety of statistical operators.

1 | INTRODUCTION

Nanofluid is an amalgam of base fluid with nanometer-sized tiny particles (size $< 10^{-6}$ mm) and this theory was presented in 1995 by Choi [1]. Choi's theory has been used in various technologies together with solar collectors [2], coating processes [3], geothermic [4], automotive engine cooling [5], biophysics [6], drug delivery [7], crystal growth [8], and rocket propellant combustion [9]. Researchers [10, 11] have classified nanoparticles into polymeric, carbides, ceramics, and metallic nanoparticles according to their chemical and physical properties. Many researchers [12–19] stated the importance of nanoparticles in industrial-level processes. Harry Williams et al. [20] investigated nanoparticles for the treatment of cancer and other infectious diseases.

Magnetohydrodynamic (MHD) study is also known as magneto-fluid dynamics in which magnetic properties of those fluids are analyzed which are electrically conducting. Electrolytes, saltwater, liquid metals, and plasmas are some common

examples of MHD fluids. MHD performed vital in astrophysics, solar physics, blood injecting machines, plasma physics, cancer tumor treatment, and MHD generators. Moreover, MHD's engineering and industrial-level applications are nuclear reactors, drug targeting, power generators, electromagnetic waves, molten salts, and plasma stability. Abbas et al. [21] inspected the transient nanofluid through a moving plate under the MHD effect. Jawad et al [22] scrutinized MHD Casson nanofluid flow with radiation impact. Thili et al. [23] examined the generation of entropy in MHD flow in nanoparticles containing base fluid. Shah et al. [24] explored MHD nanofluid flow using the HAM method. Hayat et al. [25] discussed third-grade nanofluid flow under the MHD effect. Sobamowo et al. [26] examined upper-convective Maxwell nano liquid under the MHD effect. Gupta et al. [27] analyzed Williamson nano-liquids with the MHD effect.

Heat transfer in nanofluids is an attractive field of research due to its extensive uses in aerodynamics, paint industries, medical sciences, aircraft parts production and wheel alignment. Due to various engineering and industrial-level applications, researchers have been using heat/mass transfer effects in many fluid flow models for the last few decades. Alreshidi et al. [28] discussed heat & mass transmission in 3-D nano liquid under the MHD effect. Raghunath et al. [29] examined heat along the mass transmission in a permeable media under the MHD effect. Sreedevi et al. [30] scrutinized MHD Maxwell nano liquid under heat with mass transfer. Gireesha et al. [31] scrutinized heat flow and mass transportation in Oldroyd-B type nanofluid with radiation effect.

In modern research, biologically inspired neural networks (BINNs) are used extensively in various fields such as finance, medicine, biomedical, geology, and material science to find the most accurate numerical solutions by solving real-world problems in terms of differential equations or their system. The most recent BINNs applications are, Thin-film flow [32], Painlevé-I model [33], pantograph model [34], Heart diseases prediction model [35], Ferrofluid model [36], noise interference model [37], Falkner-Skan model [38], Emden-Fowler model [39], Dengue model [40], Echo model [41], power planning [42], COVID-19 [43], Thomas-Fermi paradigm [44], wind power [45], corneal shape model [46], autoregressive control model [47], and hybrid nanofluid model [48]. As per the best of the author's knowledge, the designed solver based on inverse multiquadric radial basis function, that is, BINNs-IMQK is never yet used to solve the MHD nanofluid flow model over an exponential surface under uneven heat source/sink effects in a permeable medium. The current study's key features are:

- A newly designed solver BINNs-IMQK is constructed, using the hybridization of a "Genetic algorithms" (GAs) solver with "Sequential quadratic programming" (SQP) solver by manipulating the inverse multiquadric kernel, to solve a stiff nonlinear system of third-order nano-fluidic problem.
- The proposed BINNs-IMQK solver is quite effectively applied to scrutinize the suggested nanofluidic model for sundry scenarios.
- The validation of BINNs-IMQK solver performance is accomplished through well-known statistical operators.

The remaining part of the current research is organized as: Section 2 contains the mathematical formulation of the MHD nanofluid flow model, methodology designed for the current problem is depicted in Section 3, a comprehensive discussion of results is portrayed in Section 4, and the last section 5 is engaged for the conclusion.

2 | MATHEMATICAL FORMULATION

An incompressible 2-D MHD one-phase nanofluid unsteady flow is scrutinized over an exponentially extending sheet with a permeable media under the influence of thermophoresis and Brownian motion (see Figure 1). The flow is limited for y > 0. The unsteady form of flow starts at $t = 0$ while suction is engaged vertically to the surface. The magnetic field B is exerted normally to the direction of flow and the effects of heat sink/source as well as thermal radiation are also considered. The governing equations are [49]:

$$\frac{\partial u_1}{\partial x} + \frac{\partial u_2}{\partial y} = 0, \tag{1}$$

$$\frac{\partial u_1}{\partial t} + u_1\frac{\partial u_1}{\partial x} + u_2\frac{\partial u_2}{\partial y} = \upsilon\frac{\partial^2 u_1}{\partial y^2} - \frac{\sigma B_0^2}{\rho}u_1, \tag{2}$$

$$\frac{\partial Tm}{\partial t} + u_1\frac{\partial Tm}{\partial x} + u_2\frac{\partial Tm}{\partial y} = \alpha_{Tm}\frac{\partial^2 Tm}{\partial y^2} + \tau\left\{D_B\frac{\partial C}{\partial y}\frac{\partial Tm}{\partial y} + \frac{D_T}{Tm_\infty}\left(\frac{\partial Tm}{\partial y}\right)^2\right\} - \frac{1}{\rho C_p}\frac{\partial q_r}{\partial y} + \frac{q'''}{\rho C'_p}, \tag{3}$$

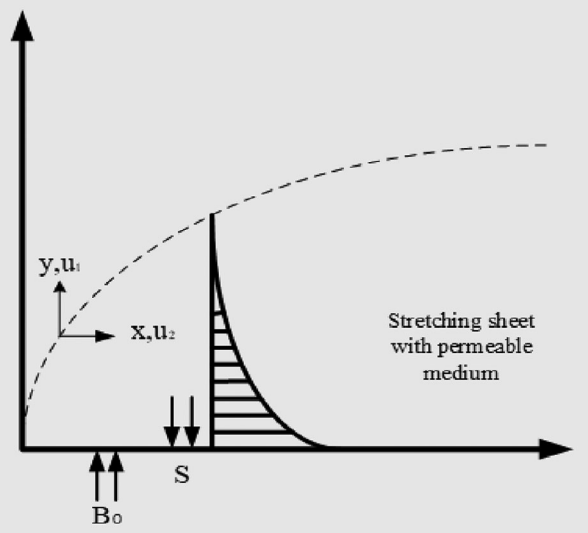

FIGURE 1 Geometrical presentation of the current problem.

$$\frac{\partial C}{\partial t}+u_1\frac{\partial C}{\partial x}+u_2\frac{\partial C}{\partial y}=D_B\frac{\partial^2 C}{\partial y^2}-\frac{D_{Tm}}{Tm_\infty}\frac{\partial^2 Tm}{\partial y^2}. \tag{4}$$

The boundary conditions are,

$$u_1=u_{1w}(x,t),\quad u_2=u_{2w}(x,t),\quad Tm=Tm_w,\quad C=C_w\quad \text{at } y=0, \tag{5}$$

$$u_1\to 0, Tm\to 0, C\to C_\infty\quad \text{when } y\to\infty. \tag{6}$$

Here $u_{1w}(x,\ t)\ =\frac{u_0}{1-\alpha_1 t}\ e^{x/L}$, $u_{2w}(x,\ t)\ =\frac{v_0}{1-\alpha_1 t}\ e^{x/2L}$ [50] with u_0 as shrinking/stretching constant and v_0 as mass suction/injection constant. The uneven heat source/sink patterned as

$$q'''=\frac{ku_{1w}}{x\upsilon}\left[A_1\left(Tm_w-Tm_\infty\right)g'+B_1\left(Tm_w-Tm_\infty\right)\right], \tag{7}$$

$$Tm_w=Tm_\infty+Tm_0\left(\frac{e^{\frac{x}{2L}}}{1-\alpha_1 t}\right), C_w=C_\infty+C_0\left(\frac{e^{\frac{x}{2L}}}{1-\alpha_1 t}\right). \tag{8}$$

The variables used in similarity transformations are

$$u_1=\frac{u_0}{1-\alpha_1 t}e^{\frac{x}{L}}g',\quad u_2=-\sqrt{\frac{u_0\upsilon}{2L\left(1-\alpha_1 t\right)}}e^{\frac{x}{2L}}\left(g+\mu g'\right),$$
$$\theta=\frac{Tm-Tm_\infty}{Tm_w-Tm_\infty},\quad \phi=\frac{C-C_\infty}{C_w-C_\infty},\quad \eta=y\sqrt{\frac{u_0}{2\upsilon L\left(1-\alpha_1 t\right)}}e^{\frac{x}{2L}}. \tag{9}$$

substitution of Equation (9) into Equations (2–6) yields

$$g'''-Mg'-2Ag'-A\eta g''-2g'^2+gg''=0, \tag{10}$$

$$\left(1+\frac{4}{3}R\right)\theta''+\Pr\left(Nb\theta'\phi'+Nt\theta'^2-2A\theta-A\eta\theta'+g'\theta-g\theta'\right)+2\left(A_1g'+B_1\theta\right)=0, \tag{11}$$

$$\phi'' + \frac{Nt}{Nb}\theta'' - Sc\left(2A\phi + A\eta\phi' + g'\phi - g\phi'\right) = 0, \tag{12}$$

along with the boundary conditions

$$g'(0) = 1,\ \ g(0) = S,\ \ \theta(0) = 1,\ \ \phi(0) = 1, \tag{13}$$

$$g'(\eta) = 0,\ \ \theta(\eta) = 0,\ \ \phi(\eta) = 0,\ \ as\ \ \eta \to \infty. \tag{14}$$

The parameters for flow used in Equations (10–12) are

$$M = \frac{\sigma B_0^2}{\rho u_0},\ \ Sc = \frac{\upsilon}{D_B},\ \ \Pr = \frac{\upsilon}{\alpha_{Tm}},\ \ R = \frac{4\sigma^* Tm_\infty^3}{kk^*},\ \ A = \frac{\alpha_1 Le^{\frac{-x}{L}}}{u_0},$$
$$Nt = \tau\frac{D_{Tm}\left(Tm_w - Tm_\infty\right)}{\upsilon Tm_\infty},\ \ Nt = \tau\frac{D_B\left(C_w - C_\infty\right)}{\upsilon},\ \ S = \upsilon_0\sqrt{\frac{2L\upsilon}{u_0(1-\alpha_1 t)}}. \tag{15}$$

3 | PROBLEM METHODOLOGY

The form of approximate solution along with its general derivative using BINNs-IMQK solver

$$\left[\hat{g}(\eta),\ \hat{\theta}(\eta), \hat{\phi}(\eta)\right] = \left(\sum_{m=1}^{n} a_{1g,m}G\left(a_{2g,m}\eta + a_{3g,m}\right),\ \sum_{m=1}^{n} a_{1\theta,m}G\left(a_{2\theta,m}\eta + a_{3\theta,m}\right),\ \sum_{m=1}^{n} a_{1\phi,m}G\left(a_{2\phi,m}\eta + a_{3\phi,m}\right)\right), \tag{16}$$

$$\left[\hat{g}^{(j)}(\eta),\ \hat{\theta}^{(j)}(\eta),\ \hat{\phi}^{(j)}(\eta)\right] = \left(\sum_{m=1}^{n} a_{1g,m}G^{(j)}\left(a_{2g,m}\eta + a_{3g,m}\right),\ \sum_{m=1}^{n} a_{1\theta,m}G^{(j)}\left(a_{2\theta,m}\eta + a_{3\theta,m}\right),\ \sum_{m=1}^{n} a_{1\phi,m}G^{(j)}\left(a_{2\phi,m}\eta + a_{3\phi,m}\right)\right). \tag{17}$$

Here a_1, a_2, and a_3 are the required weights and $\boldsymbol{W}$ represents them in vector form.

$$W = \left[W_g,\ W_\theta,\ W_\phi\right],\ \ W_g = \left[a_{1g},\ a_{2g},\ a_{3g}\right],\ \ W_\theta = \left[a_{1\theta},\ a_{2\theta},\ a_{3\theta}\right] \text{ and } W_\phi = \left[a_{1\phi},\ a_{2\phi},\ a_{3\phi}\right].$$

The required weights in components form are

$$a_{1g} = \left[a_{1g,1}, a_{1g,2}, \ldots, a_{1g,n}\right],\ \ a_{1\theta} = \left[a_{1\theta,1}, a_{1\theta,2}, \ldots, a_{1\theta,n}\right],\ \ a_{1\phi} = \left[a_{1\phi,1}, a_{1\phi,2}, \ldots, a_{1\phi,n}\right].$$

$$a_{2g} = \left[a_{2g,1}, a_{2g,2}, \ldots, a_{2g,n}\right],\ \ a_{2\theta} = \left[a_{2\theta,1}, a_{2\theta,2}, \ldots, a_{2\theta,n}\right],\ \ a_{2\phi} = \left[a_{2\phi,1}, a_{2\phi,2}, \ldots, a_{2\phi,n}\right].$$

$$a_{3g} = \left[a_{3g,1}, a_{3g,2}, \ldots, a_{3g,n}\right],\ \ a_{3\theta} = \left[a_{3\theta,1}, a_{3\theta,2}, \ldots, a_{3\theta,n}\right],\ \ a_{3\phi} = \left[a_{3\phi,1}, a_{3\phi,2}, \ldots, a_{3\phi,n}\right].$$

Here IMQ activation function $G(x) = \frac{1}{\sqrt{1+x^2}}$ [51] is utilized in BINNs-IMQK solver. The formulation of the approximate numerical solution along the derivatives is:

$$\left[\hat{g}(\eta), \hat{\theta}(\eta), \hat{\phi}(\eta)\right] = \left(\sum_{m=1}^{n}\frac{a_{1g,m}}{\sqrt{1+\left(a_{2g,m}\eta + a_{3g,m}\right)^2}},\ \sum_{m=1}^{n}\frac{a_{1\theta,m}}{\sqrt{1+\left(a_{2\theta,m}\eta + a_{3\theta,m}\right)^2}},\ \sum_{m=1}^{n}\frac{a_{1\phi,m}}{\sqrt{1+\left(a_{2\phi,m}\eta + a_{3\phi,m}\right)^2}}\right), \tag{18}$$

$$\hat{g}'''(\eta) = \sum_{m=1}^{n}\left[a_{1g,m}a_{2g,m}^{3}\left(\frac{9\left(a_{2g,m}\eta + a_{3g,m}\right)}{\left(1+\left(a_{2g,m}\eta + a_{3g,m}\right)^{2}\right)^{\frac{5}{2}}} - \frac{15\left(a_{2g,m}\eta + a_{3g,m}\right)^{3}}{\left(1+\left(a_{2g,m}\eta + a_{3g,m}\right)^{2}\right)^{\frac{7}{2}}}\right)\right], \tag{19}$$

$$\hat{\theta}''(\eta) = \sum_{m=1}^{n}\left[a_{1\theta,m}a_{2\theta,m}^{2}\left(\frac{-1+2\left(a_{2\theta,m}\eta + a_{3\theta,m}\right)^{2}}{\left(1+\left(a_{2\theta,m}\eta + a_{3\theta,m}\right)^{2}\right)^{\frac{5}{2}}}\right)\right], \tag{20}$$

$$\hat{\phi}''(\eta) = \sum_{m=1}^{n}\left[a_{1\phi,m}a_{2\phi,m}^{2}\left(\frac{-1+2\left(a_{2\phi,m}\eta + a_{3\phi,m}\right)^{2}}{\left(1+\left(a_{2\phi,m}\eta + a_{3\phi,m}\right)^{2}\right)^{\frac{5}{2}}}\right)\right]. \tag{21}$$

The mathematical formulation of the fitness function is,

$$E_{11} = \frac{1}{r}\sum_{l=1}^{r}\left(\hat{g'''}_{l} - M\hat{g'}_{l} - 2A\hat{g'}_{l} - A\eta\hat{g''}_{l} - 2\hat{g'}_{l}^{2} + \hat{g}_{l}\hat{g''}_{l}\right)^{2}, \tag{22}$$

$$E_{22} = \frac{1}{r}\sum_{l=1}^{r}\left(\left(\left(1+\frac{4}{3}R\right)\hat{\theta''}_{l} + 2\left(A_{1}\hat{g'}_{l} + B_{1}\hat{\theta}_{l}\right) + \Pr\left(Nb\hat{\theta'}_{l}\hat{\phi'}_{l} + Nt\,\hat{\theta}_{l}'^{2} - 2A\hat{\theta}_{l} - A\eta\hat{\theta}_{l}' + \hat{g'}_{l}\hat{\theta}_{l} - \hat{g}_{l}\hat{\theta}_{l}'\right)\right)^{2}, \tag{23}$$

$$E_{33} = \frac{1}{r}\sum_{l=1}^{r}\left(\hat{\phi''}_{l} + \frac{Nt}{Nb}\hat{\theta''}_{l} - Sc\left(2A\hat{\phi}_{l} + \hat{g'}_{l}\hat{\phi}_{l} + A\eta\hat{\phi'}_{l} - \hat{g}_{l}\hat{\phi'}_{l}\right)\right)^{2}, \tag{24}$$

$$E_{00} = \frac{1}{7}\left[\left(\hat{g}_{1} - S\right)^{2} + \left(\hat{g}_{1}' - 1\right)^{2} + \left(\hat{\theta}_{1} - 1\right)^{2} + \left(\hat{\phi}_{1} - 1\right)^{2} + \hat{g'}_{r}^{2} + \hat{\phi}_{r}^{2} + \hat{\theta}_{r}^{2}\right], \tag{25}$$

$$E = E_{00} + E_{11} + E_{22} + E_{33}. \tag{26}$$

Here Equation 25 represents the boundary conditions given in the Equations (13 and 14) while Equation 26 represents the formation of the fitness function using the BINNs-IMQK solver.

3.1 | Optimization networks

The hybrid process in the current research is completed via GAs and SQP is used for functioning of BINNs-IMQK solver. The structural diagram of BINNs-IMQK to solve the suggested MHD nanofluid flow model in terms of a nonlinear ODEs system is portrayed in Figure 2.

3.1.1 | Genetic algorithm (GAs)

GA is a well-known global solver which was introduced in 1970 by J. Holland. GAs work on a randomly stimulated population to obtain the most suitable or improved approximations. Individuals are sorted out in the case of each generation, through a stream of a quite new population depending upon fitness level after which the variation operators are applied.

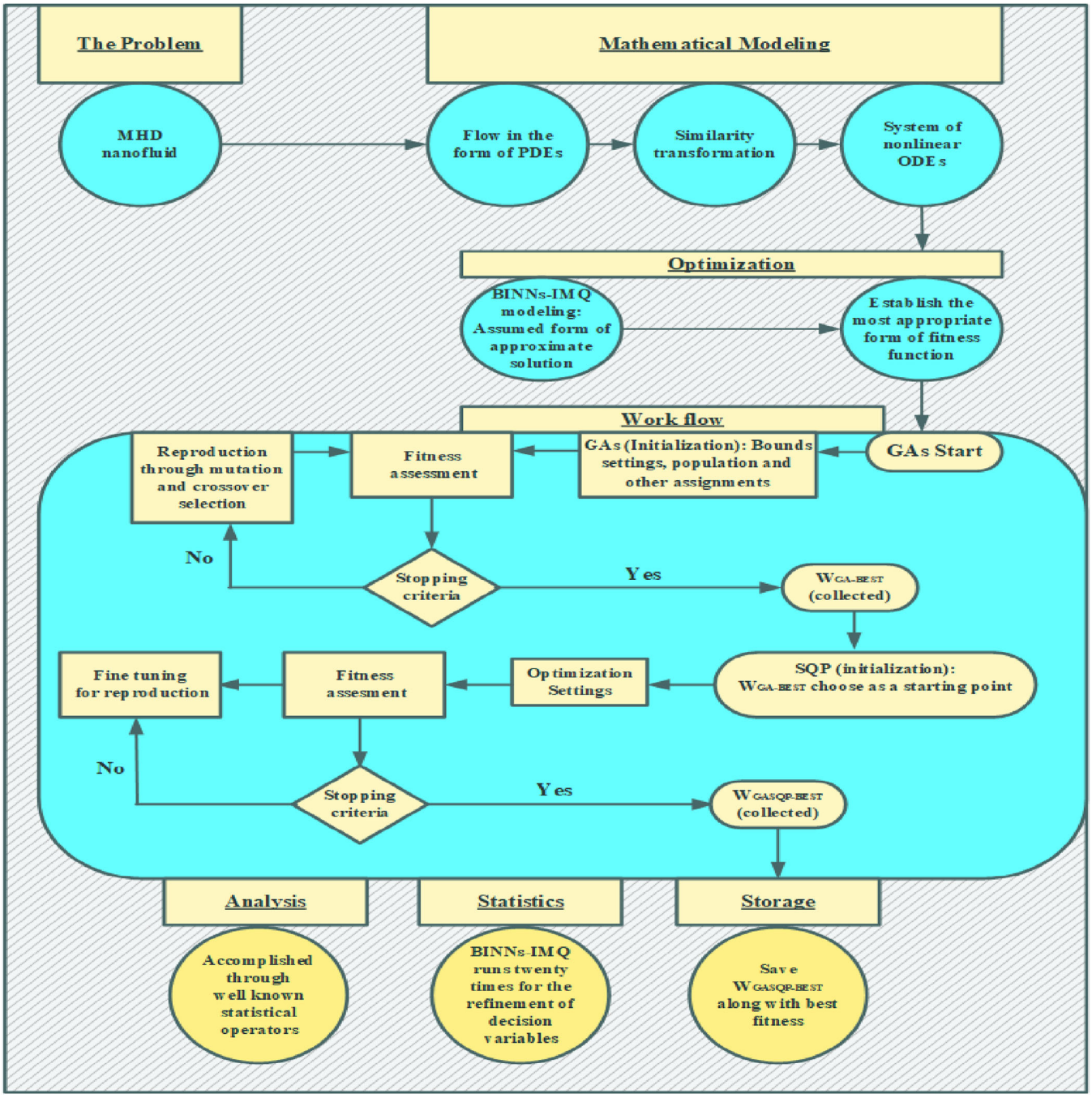

FIGURE 2 MHD nanofluidic model detailed form graphical abstract manufactured using BINNs-IMQK solver.

The key features of GAs functioning depend on quite reliable values of elitism, mutation, and crossover with selection. The most recent research in which GAs performed a key role is given in [52–56].

3.1.2 | Sequential quadratic programming (SQP)

The hybridization process through an effective local search solver is a technique normally adopted for GAs to achieve fast optimization of problem-specific parameters. Presently, SQP is selected for this task. SQP is familiar because of its effectiveness and speedy convergence. Some recent applications of SQP are [57–59]. Algorithm 1 portrayed the pseudocode of this GA-SQP hybridization for the application of the BINNs-IMQK solver.

ALGORITHM 1 BINNs-IMQK algorithm in terms of pseudocode for suggested problem.

GAs process(%start%)

Inputs: Chromosomes portray as:

$W = [W_g, W_\theta, W_\phi], W_g = [a_{1g}, a_{2g}, a_{3g}], W_\theta = [a_{1\theta}, a_{2\theta}, a_{3\theta}]$ and $W_\phi = [a_{1\phi}, a_{2\phi}, a_{3\phi}]$

The components used in weight vector "***W***" are

$a_{1g} = [a_{1g,1}, a_{1g,2}, \ldots, a_{1g,n}]$, $a_{1\theta} = [a_{1\theta,1}, a_{1\theta,2}, \ldots, a_{1\theta,n}]$, $a_{1\phi} = [a_{1\phi,1}, a_{1\phi,2}, \ldots, a_{1\phi,n}]$

$a_{2g} = [a_{2g,1}, a_{2g,2}, \ldots, a_{2g,n}]$, $a_{2\theta} = [a_{2\theta,1}, a_{2\theta,2}, \ldots, a_{2\theta,n}]$, $a_{2\phi} = [a_{2\phi,1}, a_{2\phi,2}, \ldots, a_{2\phi,n}]$

$a_{3g} = [a_{3g,1}, a_{3g,2}, \ldots, a_{3g,n}]$, $a_{3\theta} = [a_{3\theta,1}, a_{3\theta,2}, \ldots, a_{3\theta,n}]$, $a_{3\phi} = [a_{3\phi,1}, a_{3\phi,2}, \ldots, a_{3\phi,n}]$

Output: Optimization to collect GAs best weights i-e, $\boldsymbol{W_{BEST\text{-}GA}}$.

Initialization: Selection of chromosomes by adjusting the weight vector.

Fitness computation: Customize "E" using equations (22–26) for each vector included in the population.

Stopping criteria: stop when any of the following conditions are attained:

Generation → 400, Tol.function, fit-limit → $1e^{-11}$, Stall-Gen → 111, Elite-count → 50, Ini-pop → 200, Other selections (By default)

Ranking: Rank the specific weight vector in the assigned population-based fitness values.

Storage: $\mathbf{W_{GA\text{-}Best}}$, Iterations along function count and fitness.

GA process accomplished

SQP (start)

Inputs: Take $\mathbf{W_{GA\text{-}Best}}$ as a starting point.

Initialization: $\mathbf{W_{GA\text{-}Best}}$ along with assignments and generations.

Stopping Conditions: Terminate the SQP hybridization process if any of the following conditions are achieved.

Max-fun → 11,00,000, Tol-fun, Tol-X → $1e^{-11}$, Max-Ite → 1111.

Evaluation of Fitness: Analyze the values of "**E**" and "**W**" for system of Equations (22–26).

Adjustment: Fine-tuning of "fmincon" for "**W**".

Storage: Accumulate **"E",** $\mathbf{W_{GASQP\text{-}Best}}$ along with iterations and function count.

SQP End

Data productions

Repeat the process to complete twenty runs and through BINNs-IMQK solver, use this data for best numerical outcomes for the system of non-linear ODEs.

TABLE 1 List of physical parameters along their assigned values.

Scenarios	Parameters	C −1	C −2	C −3	C −4
	A	1.25	1.71	2.40	3.25
	Nb	0.10	0.40	0.70	1.05
	S	0	1.20	2.40	3.60
	R	0	1.25	2.50	3.75
	Sc	0.35	0.50	0.65	0.85
	Pr	2.01	3.01	4.05	5.55

3.2 | Performance matrix

BINNs-IMQK solver performance is scrutinized via statistical performance operators (RMSE, E-TIC E-NSE, E-R^2, and E-VAF).

$$\begin{bmatrix} R^2_{\bar{g}} \\ R^2_{\bar{\theta}} \\ R^2_{\bar{\phi}} \end{bmatrix} = \begin{bmatrix} \frac{SS_{reg:g}}{SS_{total:g}} \\ \frac{SS_{reg:\theta}}{SS_{total:\theta}} \\ \frac{SS_{reg:\phi}}{SS_{total:\phi}} \end{bmatrix}, \quad \begin{bmatrix} RMSE_{\hat{g}} \\ RMSE_{\hat{\theta}} \\ RMSE_{\hat{\phi}} \end{bmatrix} = \begin{bmatrix} \sqrt{\frac{1}{n}\sum_{s=1}^{n}\left(\hat{g}_s - g_{ref:s}\right)^2} \\ \sqrt{\frac{1}{n}\sum_{s=1}^{n}\left(\hat{\theta}_s - \theta_{ref:s}\right)^2} \\ \sqrt{\frac{1}{n}\sum_{s=1}^{n}\left(\hat{\phi}_s - \phi_{ref:s}\right)^2} \end{bmatrix}_{NF}, \quad \begin{bmatrix} VAF_{\hat{g}} \\ VAF_{\hat{\theta}} \\ VAF_{\hat{\phi}} \end{bmatrix} = \begin{bmatrix} \left(1 - \frac{var(g_{ref:s} - \hat{g}_s)}{var(g_s)}\right) \times 100 \\ \left(1 - \frac{var(\theta_{ref:s} - \hat{\theta}_s)}{var(\theta_s)}\right) \times 100 \\ \left(1 - \frac{var(\phi_{ref:s} - \hat{\phi}_s)}{var(\phi_s)}\right) \times 100 \end{bmatrix}_{NF},$$

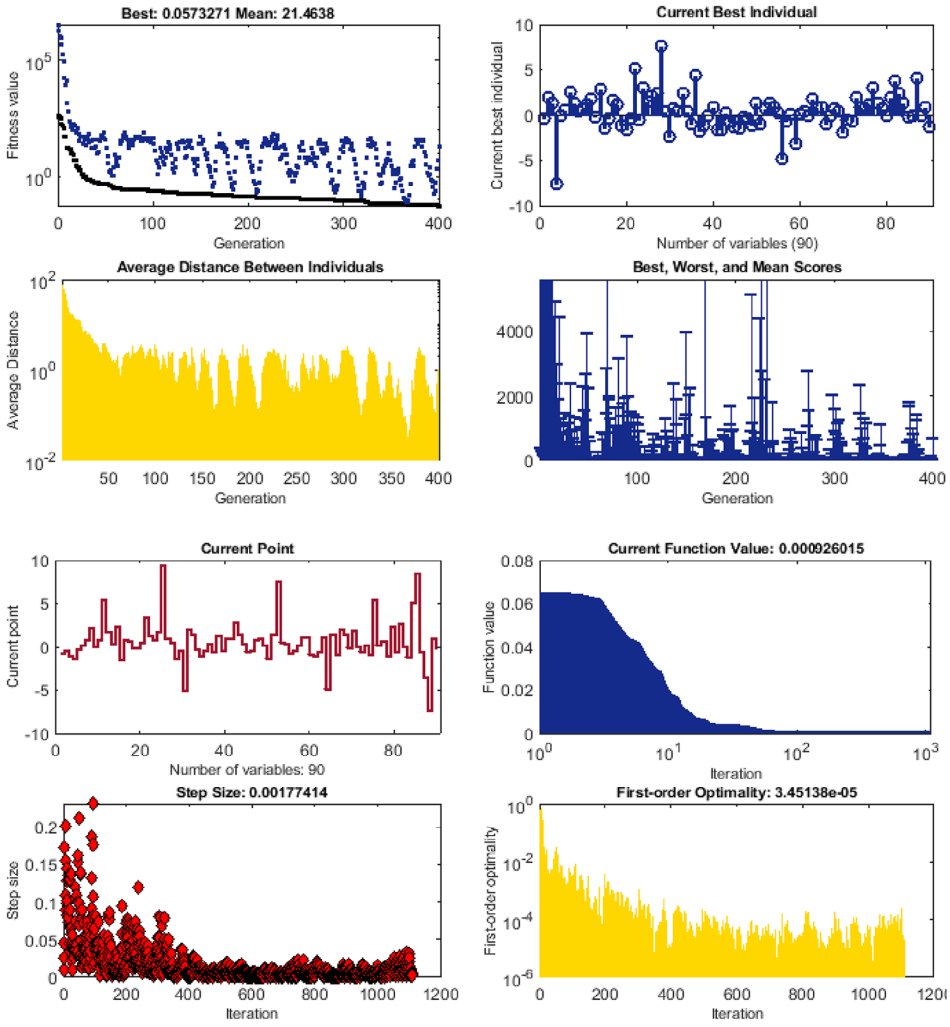

FIGURE 3 Graphs of learning curves in first case of scenario-I acquired using BINNs-IMQK solver.

$$\begin{bmatrix} E-VAF_{\hat{g}} \\ E-VAF_{\hat{\theta}} \\ E-VAF_{\hat{\phi}} \end{bmatrix} = \begin{bmatrix} 100-VAF_{\hat{g}} \\ 100-VAF_{\hat{\theta}} \\ 100-VAF_{\hat{\phi}} \end{bmatrix}_{NF},$$

$$\begin{bmatrix} E-R^2_{\hat{g}} \\ E-R^2_{\hat{\theta}} \\ E-R^2_{\hat{\phi}} \end{bmatrix} = \begin{bmatrix} 1-R^2_{\hat{g}} \\ 1-R^2_{\hat{\theta}} \\ 1-R^2_{\hat{\phi}} \end{bmatrix}_{NF} \quad \begin{bmatrix} NSE_{\hat{g}} \\ NSE_{\hat{\theta}} \\ NSE_{\hat{\phi}} \end{bmatrix} = \begin{bmatrix} 1-\frac{\sum_{s=1}^{n}\left(\hat{g}_s-g_{ref:s}\right)^2}{\sum_{s=1}^{n}\left(\hat{g}_s-\overline{g_s}\right)^2} \\ 1-\frac{\sum_{s=1}^{n}\left(\hat{\theta}_s-\theta_{ref:s}\right)^2}{\sum_{s=1}^{n}\left(\hat{\theta}_s-\overline{\theta_s}\right)^2} \\ 1-\frac{\sum_{s=1}^{n}\left(\hat{\phi}_s-\phi_{ref:s}\right)^2}{\sum_{s=1}^{n}\left(\hat{\phi}_s-\overline{\phi_s}\right)^2} \end{bmatrix}_{NF}, \begin{bmatrix} TIC_{\hat{g}} \\ TIC_{\hat{\theta}} \\ TIC_{\hat{\phi}} \end{bmatrix} = \begin{bmatrix} \frac{\sqrt{\frac{1}{n}\sum_{s=1}^{n}\left(\hat{g}_s-g_{ref:s}\right)^2}}{\sqrt{\frac{1}{n}\sum_{s=1}^{n}\hat{g}_s^2}+\sqrt{\frac{1}{n}\sum_{s=1}^{n}g^2_{ref:s}}} \\ \frac{\sqrt{\frac{1}{n}\sum_{s=1}^{n}\left(\hat{\theta}_s-\theta_{ref:s}\right)^2}}{\sqrt{\frac{1}{n}\sum_{s=1}^{n}\hat{\theta}_s^2}+\sqrt{\frac{1}{n}\sum_{s=1}^{n}\theta^2_{ref:s}}} \\ \frac{\sqrt{\frac{1}{n}\sum_{s=1}^{n}\left(\hat{\phi}_s-\phi_{ref:s}\right)^2}}{\sqrt{\frac{1}{n}\sum_{s=1}^{n}\hat{\phi}_s^2}+\sqrt{\frac{1}{n}\sum_{s=1}^{n}\phi^2_{ref:s}}} \end{bmatrix}_{NF},$$

$$\begin{bmatrix} E-NSE_{\hat{g}} \\ E-NSE_{\hat{\theta}} \\ E-NSE_{\hat{\phi}} \end{bmatrix} = \begin{bmatrix} 1-NSE_{\hat{g}} \\ 1-NSE_{\hat{\theta}} \\ 1-NSE_{\hat{\phi}} \end{bmatrix}_{NF}$$

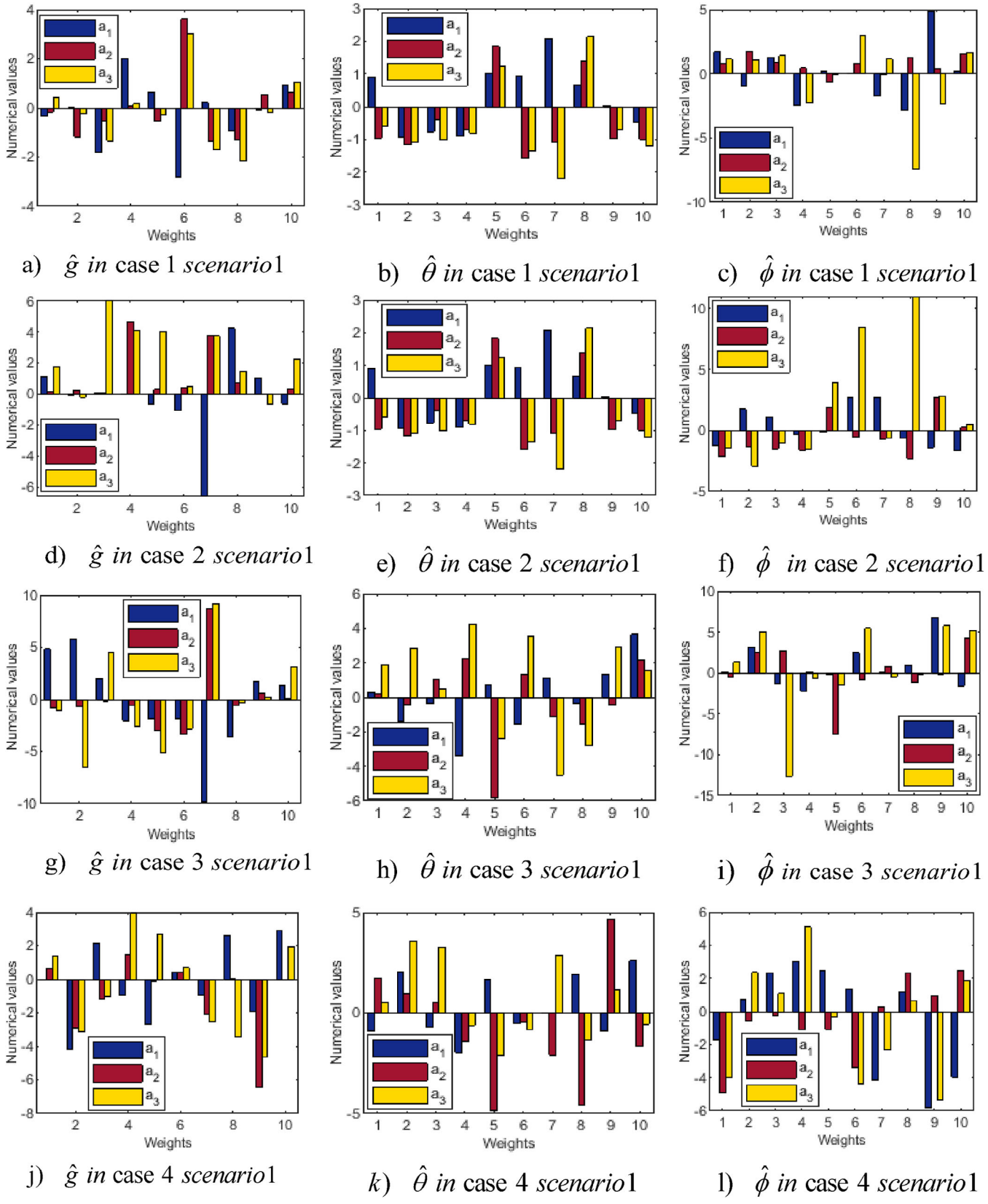

FIGURE 4 Best weights in MHD nanofluid flow model for all cases of scenario 1.

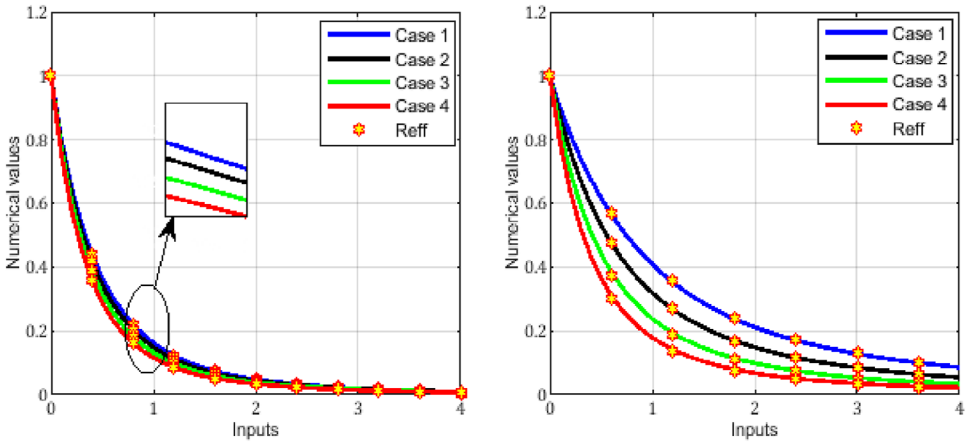

a) Numerical values for $\hat{g}'(\eta)$ b) Numerical values for $\hat{\theta}(\eta)$

FIGURE 5 Numerical values obtained in MHD nanofluid flow model for scenario 1.

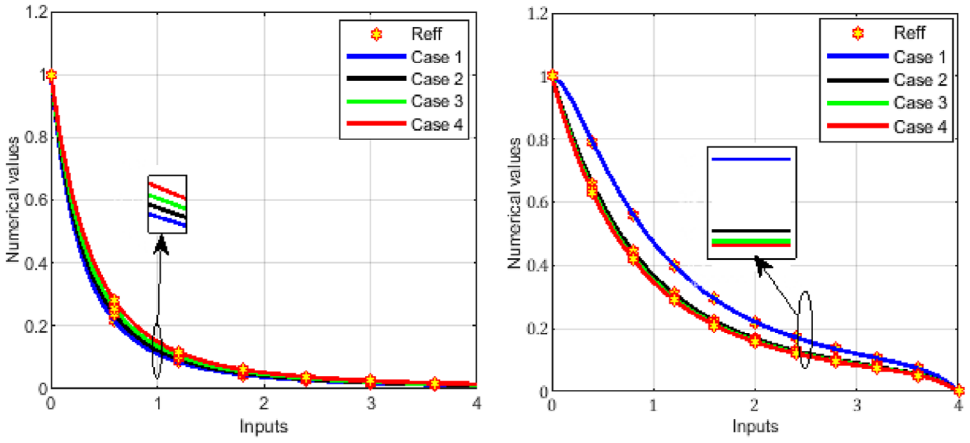

a) Numerical values for temperature b) Numerical values for mass concentration

FIGURE 6 Numerical values obtained in MHD nanofluid flow model for scenario 2.

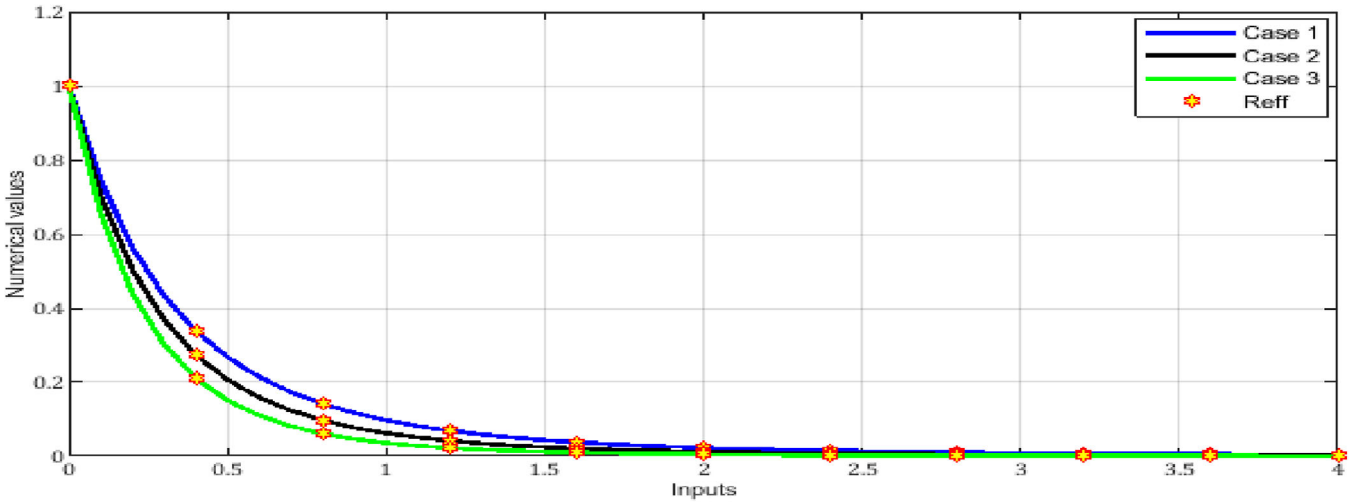

a) Numerical values for $\hat{g}'(\eta)$

FIGURE 7 Numerical values obtained in MHD nanofluid flow model for scenario 3.

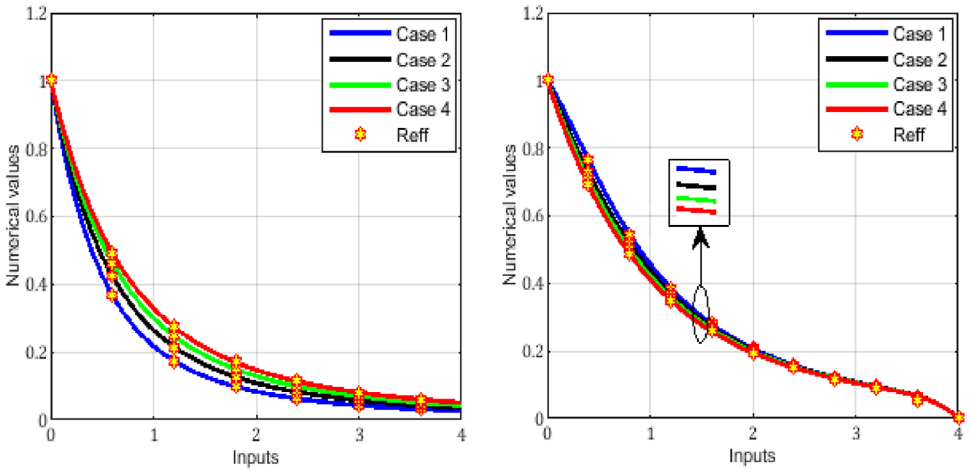

a) Numerical values for $\hat{\theta}(\eta)$ b) Numerical values for $\hat{\phi}(\eta)$

FIGURE 8 Numerical values obtained in MHD nanofluid flow model for scenario 4.

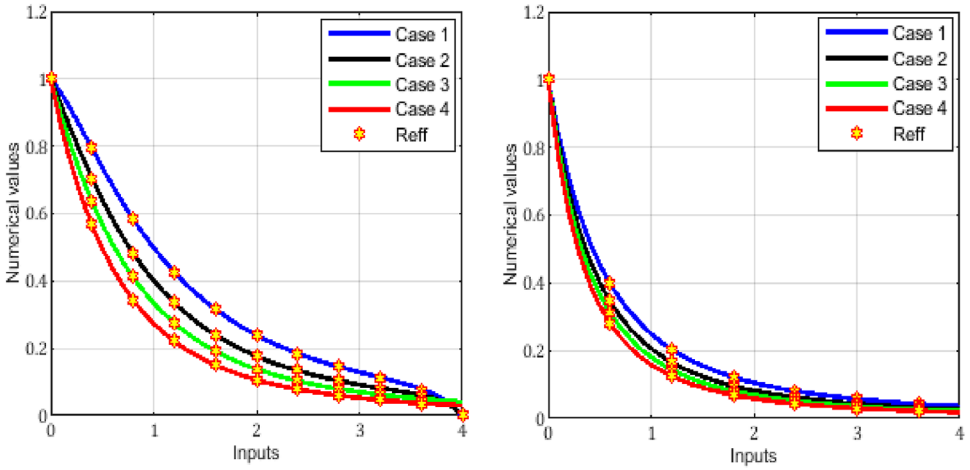

a) Numerical values for $\hat{\phi}(\eta)$ Scenario 5 b) Numerical values for $\hat{\theta}(\eta)$ Scenario 6

FIGURE 9 Numerical values obtained in suggested nanofluidic model for scenarios (5-6).

4 | RESULTS AND DISCUSSION

The suggested MHD nanofluid problem over an exponentially stretchable sheet in a permeable media is solved numerically by BINNs-IMQK solver which ran 20 times with appropriate optim-setting for six different scenarios constructed through different values assigned to physical parameters listed in Table 1. The required weights for the solution of the current problem are trained using the proposed solver and the obtained learning curves for Case 1(for scenario 1) are depicted in Figure 3. The trained weights in all cases (for scenario 1) are graphically illustrated in Figure 4. The weights obtained for all six scenarios are finally substituted in Equation 16 to obtain the solution of MHD nanofluid problem.

The numerical outcomes for velocity profile $\hat{g}'(\eta)$, thermal gradient $\hat{\theta}(\eta)$, and nanofluidic concentration profile $\hat{\phi}(\eta)$ are obtained and graphically depicted in Figures 5–9. Figure 5 portrays variation in $\hat{g}'(\eta)$ and $\hat{\theta}(\eta)$ due to unsteady parameter (A). The values of $\hat{g}'(\eta)$ and $\hat{\theta}(\eta)$ of the nanofluid reduce with an escalation in the value of A. The decrease in the values of $\hat{g}'(\eta)$ and $\hat{\theta}(\eta)$ is due to the reduction in the velocity along the stretching sheet with the increase in A and very small amount of heat is transferred from nanofluid to the sheet. Figure 6 shows variation in $\hat{\theta}(\eta)$ and $\hat{\phi}(\eta)$ due to the Brownian motion parameter (Nb). The temperature of MHD nanofluid inflates with the rise in the value of Nb as the Brownian motion plays a vital role in strengthening the nanofluid's thermal conductivity due to which collision between nanoparticles rises

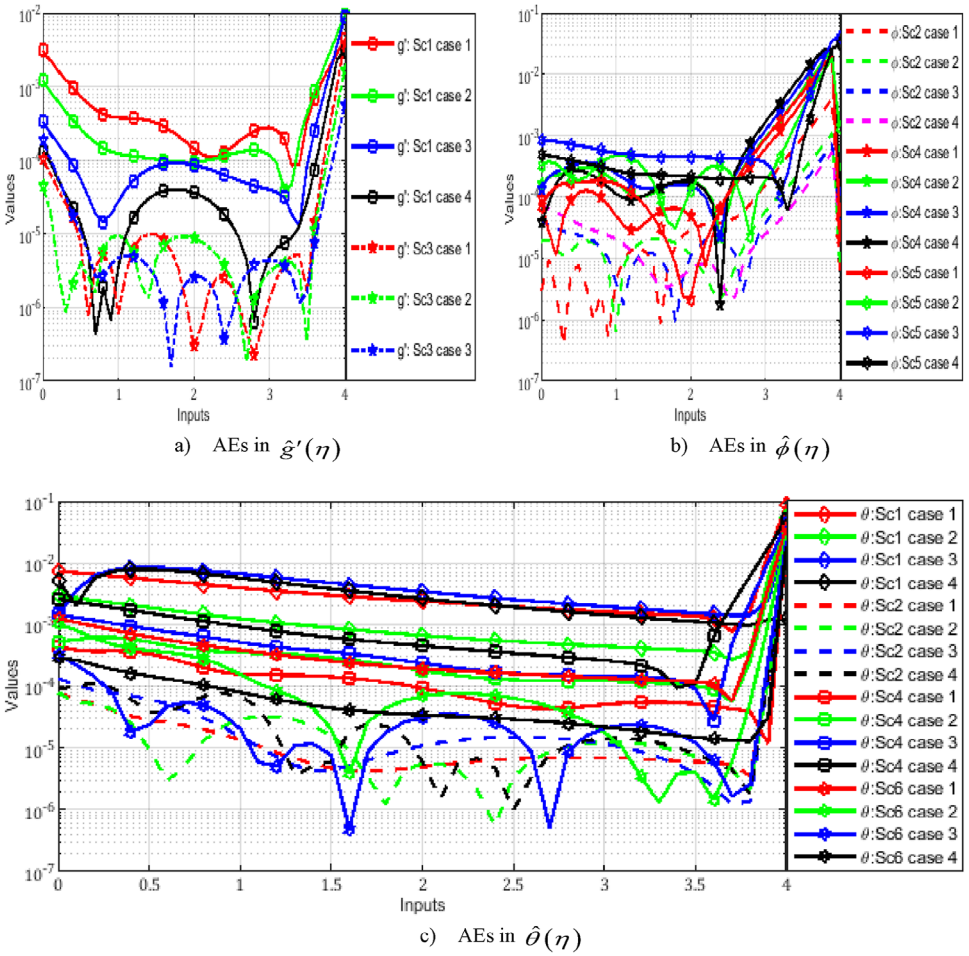

FIGURE 10 Calculated values of AEs in MHD nanofluid flow model for all scenarios.

within the fluid and as a result concentration decrease. Figure 7 illustrates the consequences of the suction parameter (S) on velocity $\hat{g}'(\eta)$. It appears that the velocity value is depressed with the increase in the value of S as it resists the fluid flow. Figure 8 portrays the impression of radiation parameter (R) on $\hat{\theta}(\eta)$ and $\hat{\phi}(\eta)$. The uplift value of R enhances the nanofluidic temperature as the larger value of R releases a huge amount of heat energy and temperature escalates which enhances the collision within the fluid and as a result concentration of nanoparticles diminishes. The first part of Figure 9 illustrates the influence of the Schmidt number (Sc) on the value of $\hat{\phi}(\eta)$. The increase in the value of Sc diminishes the motion of nanoparticles that boosts the concentration of fluid. The second part of Figure 9 describes the significance of Prandtl number (Pr) on $\hat{\theta}(\eta)$. The larger value of Pr reduces the fluid temperature as a larger value of Pr inflates the kinematic viscosity of nanofluid and so temperature reduces.

The results of the suggested problem obtained through BINNs-IMQK solver overlap the reference solution calculated through the Adams method on [0, 4] interval for all six scenarios. Figure 10 illustrates the matching degree of BINNs-IMQK solver through absolute errors (AEs) and shows that the range of AEs in all scenarios is 10^{-2} to 10^{-7} for $\hat{g}'(\eta)$, 10^{-1} to 10^{-7} for $\hat{\theta}(\eta)$, and $\hat{\phi}(\eta)$ which proves the accuracy of BINNs-IMQK solver. Table 2 depicts the values of AEs in the tabulated form of some equally spaced arguments on the interval [0, 4].

BINNs-IMQK solver performance is inspected by exploiting the statistical operators namely E-VAF, NSEE, RMSE, E-R^2, E-TIC, and MAE are illustrated in Figures 11–13 for different scenarios. Figure 11 elucidated the E-VAF analysis for all scenarios and depicts the range of accuracy for scenarios 1, 4, 5, and 6 from 10^{-2} to 10^{-8}, scenario 2 from 10^{-2} to 10^{-10} and scenario 3 from 10^{-5} to 10^{-8}. Figure 12 presented the E-NSE analysis and portrays the range of accuracy for scenarios 1, 4, and 5 from 10^{-2} to 10^{-6}, scenario 2 from 10^{-2} to 10^{-8}, scenario 3 from 10^{-3} to 10^{-7}, and scenario 6 from 10^{-3} to 10^{-6}.

TABLE 2 AEs in tabulated form for all six scenarios of nanofluidic model.

Scenario-I								
	$\hat{g}'(\eta)$				$\hat{\theta}(\eta)$			
η	**C- 1**	**C −2**	**C −3**	**C −4**	**C- 1**	**C −2**	**C −3**	**C −4**
0	3.10E-3	1.20E-3	4.24E-4	2.52E-4	7.25E-3	2.94E-3	1.11E-3	1.21E-3
0.5	7.52E-4	2.68E-4	8.45E-5	4.39E-5	5.35E-3	1.88E-3	8.40E-3	9.18E-3
1.0	3.58E-4	1.14E-4	4.46E-5	3.24E-5	3.93E-3	1.25E-3	6.65E-3	6.31E-3
1.5	3.27E-4	1.04E-4	3.84E-5	4.93E-5	2.99E-3	8.89E-4	4.74E-3	4.14E-3
2.0	3.22E-4	1.19E-4	4.89E-5	5.54E-5	2.36E-3	6.72E-4	3.42E-3	2.84E-3
2.5	3.02E-4	1.27E-4	5.09E-5	4.21E-5	1.93E-3	5.33E-4	2.55E-3	2.05E-3
3.0	1.38E-4	9.13E-5	5.78E-5	4.82E-5	1.62E-3	4.41E-4	1.96E-3	1.55E-3
3.5	9.74E-4	4.36E-4	7.59E-5	2.94E-5	1.37E-3	3.74E-4	1.54E-3	1.20E-3
4.0	9.16E-3	9.60E-3	8.90E-3	2.91E-3	8.56E-2	5.45E-2	3.32E-2	1.31E-3
Scenario 2								
	$\hat{\theta}(\eta)$				$\hat{\phi}(\eta)$			
η	**C- 1**	**C −2**	**C −3**	**C −4**	**C- 1**	**C −2**	**C −3**	**C −4**
0	8.39E-4	2.63E-4	2.91E-4	2.13E-4	1.53E-3	9.18E-4	1.36E-3	8.09E-4
0.5	1.86E-4	9.59E-5	1.24E-4	1.30E-4	1.17E-3	5.48E-4	8.97E-4	4.58E-4
1.0	7.66E-5	4.18E-5	5.70E-5	6.13E-5	9.43E-4	4.93E-4	7.33E-4	3.86E-4
1.5	4.18E-5	2.79E-5	3.11E-5	3.23E-5	9.67E-4	5.57E-4	7.55E-4	4.77E-4
2.0	2.40E-5	2.30E-5	1.84E-5	2.43E-5	1.03E-3	5.58E-4	7.45E-4	4.95E-4
2.5	1.91E-5	1.80E-5	1.28E-5	1.87E-5	9.25E-4	5.07E-4	7.13E-4	3.45E-4
3.0	1.58E-5	1.19E-5	1.14E-5	1.53E-5	2.99E-4	1.87E-4	2.01E-4	1.52E-4
3.5	1.14E-5	9.67E-6	9.78E-6	1.21E-5	4.45E-3	2.17E-3	3.11E-3	1.72E-3
4.0	1.10E-2	1.23E-2	1.36E-2	1.52E-2	3.06E-2	1.64E-2	2.53E-2	1.38E-2
Scenario 3								
	$\hat{g}(\eta)$				$\hat{g}'(\eta)$			
η	**C- 1**	**C −2**	**C −3**	**C −4**	**C- 1**	**C −2**	**C −3**	**C −4**
0	9.03E-4	4.63E-4	6.28E-4	4.40E-4	2.16E-4	3.37E-4	1.01E-3	5.07E-4
0.5	9.96E-4	5.01E-4	6.88E-4	6.71E-5	3.07E-5	3.01E-5	1.02E-3	5.21E-4
1.0	1.01E-3	5.07E-4	6.96E-4	2.27E-5	5.59E-5	3.96E-5	1.03E-3	5.32E-4
1.5	1.02E-3	5.21E-4	7.11E-4	2.22E-5	4.79E-5	3.63E-5	1.03E-3	5.41E-4
2.0	1.03E-3	5.32E-4	7.17E-4	1.67E-5	4.33E-5	3.50E-5	1.02E-3	5.45E-4
2.5	1.03E-3	5.41E-4	7.15E-4	1.47E-5	3.49E-5	3.45E-5	1.02E-3	5.43E-4
3.0	1.02E-3	5.45E-4	7.12E-4	1.48E-5	3.45E-5	3.59E-5	1.15E-3	5.39E-4
3.5	1.02E-3	5.43E-4	7.10E-4	1.20E-5	2.62E-5	2.16E-5	1.15E-3	5.39E-4
4.0	1.15E-3	5.39E-4	6.56E-4	3.91E-3	1.63E-3	5.73E-4	2.19E-3	2.92E-3
Scenario 4								
	$\hat{\theta}(\eta)$				$\hat{\phi}(\eta)$			
η	**C- 1**	**C −2**	**C −3**	**C −4**	**C- 1**	**C −2**	**C −3**	**C −4**
0	2.19E-3	2.92E-3	3.30E-3	3.95E-3	1.29E-3	1.87E-3	1.22E-3	1.16E-3
0.5	1.05E-3	1.50E-3	1.81E-3	2.25E-3	1.12E-3	1.38E-3	1.21E-3	1.20E-3
1.0	5.56E-4	8.37E-4	1.07E-3	1.37E-3	9.70E-4	1.10E-3	1.05E-3	1.09E-3
1.5	3.35E-4	5.27E-4	6.88E-4	9.01E-4	9.03E-4	9.63E-4	1.02E-3	9.82E-4
2.0	2.21E-4	3.57E-4	4.71E-4	6.28E-4	8.50E-4	9.29E-4	9.77E-4	9.07E-4
2.5	1.56E-4	2.56E-4	3.42E-4	4.65E-4	8.03E-4	8.27E-4	7.58E-4	7.21E-4
3.0	1.18E-4	1.94E-4	2.64E-4	3.58E-4	3.30E-4	6.02E-4	9.02E-4	1.35E-3
3.5	9.61E-5	1.57E-4	1.79E-4	6.03E-5	7.06E-3	9.15E-3	1.12E-2	1.35E-2
4.0	2.65E-2	3.55E-2	4.35E-2	5.09E-2	3.48E-2	3.76E-2	3.63E-2	3.49E-2

(Continues)

TABLE 2 (Continued)

	Scenario 5				Scenario 6			
	$\hat{\phi}(\eta)$				$\hat{\theta}(\eta)$			
η	C- 1	C −2	C −3	C −4	C- 1	C −2	C −3	C −4
0	1.73E-3	1.41E-3	8.58E-4	4.91E-4	1.29E-3	1.01E-3	7.20E-4	4.83E-4
0.5	1.56E-3	1.18E-3	6.92E-4	3.74E-4	6.49E-4	4.42E-4	2.77E-4	1.88E-4
1.0	1.34E-3	9.37E-4	5.30E-4	2.77E-4	3.89E-4	2.56E-4	1.49E-4	9.65E-5
1.5	1.33E-3	8.86E-4	4.60E-4	2.28E-4	2.63E-4	1.50E-4	8.78E-5	5.70E-5
2.0	1.28E-3	8.57E-4	4.35E-4	2.10E-4	2.00E-4	1.01E-4	6.17E-5	3.86E-5
2.5	1.03E-3	8.03E-4	4.43E-4	2.10E-4	1.62E-4	7.61E-5	4.64E-5	2.87E-5
3.0	6.54E-4	3.61E-4	3.59E-4	2.04E-4	1.36E-4	6.41E-5	3.65E-5	2.32E-5
3.5	9.55E-3	5.03E-3	2.16E-3	6.90E-4	1.22E-4	5.81E-5	2.97E-5	1.96E-5
4.0	3.95E-2	4.910E-2	4.12E-2	3.080E-2	3.66E-2	2.72E-2	2.240E-2	1.86E-2

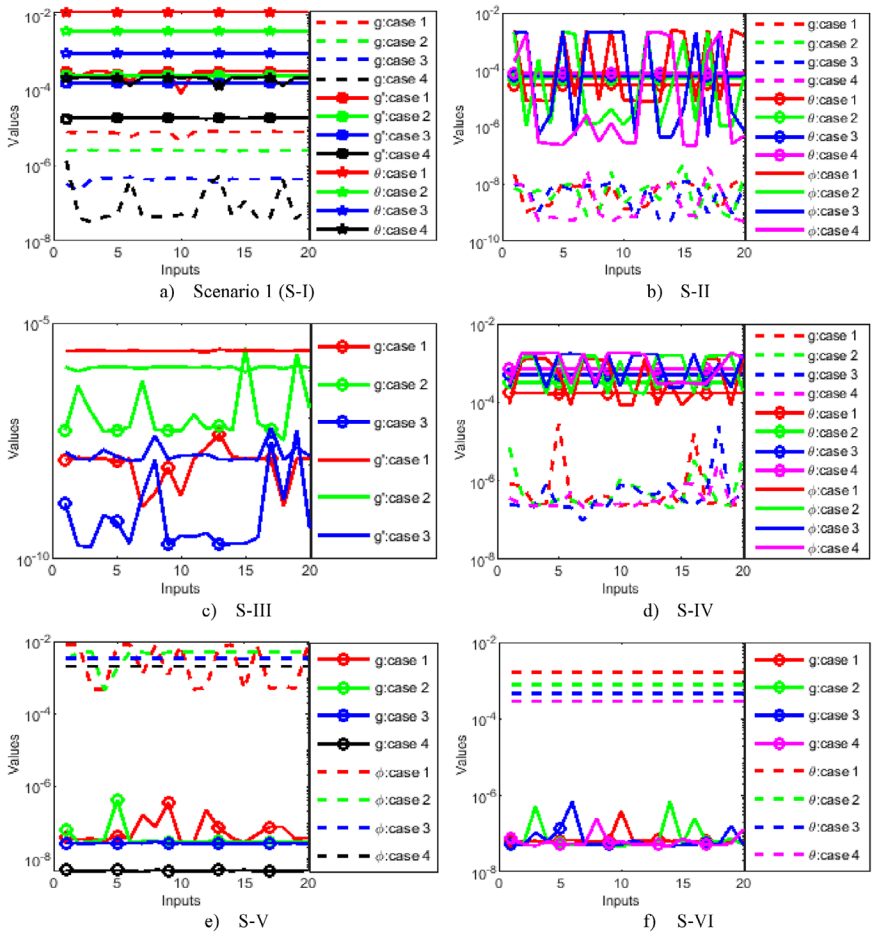

FIGURE 11 E-VAF analysis for all scenarios in MHD nanofluid flow model.

Figure 13 displayed the statistical analysis for some randomly taken scenarios that shows the range of accuracy for (RMSE) scenario 3 from 10^{-3} to 10^{-4}, (E-R^2) scenario 4 from 10^{-1} to 10^{-7}, (E-TIC) scenario 5 from 10^{-2} to 10^{-5}, and (MAE) scenario 6 from 10^{-3} to 10^{-4}. All these results are nearly equal to zero which proves BINNs-IMQK solver is a quite reliable method. Moreover, the fitness of BINNs-IMQK solver is examined through CDF plot analysis and histogram and presented here for scenario 3 through Figures 14–17. Figure 14 shows the fitness in all cases of S-III in terms of area and the accuracy obtained lies in a range of 10^{-3} to 10^{-4}. Figure 15 expresses the fitness in terms of CDF analysis in cases C (I-III) of S-III and acquired an accuracy range of 10^{-3} to 10^{-4}. Figure 16 illustrates the histogram analysis in all three cases of the third scenario and shows that almost 60% of the runs obtained an accuracy range of 10^{-3} to 10^{-4}. Figure 17a demonstrates the fitness in terms of a sorted chart using VAF in all cases of S-III and shows a range of 10^{-5} to 10^{-10} (up to 9 decimals).

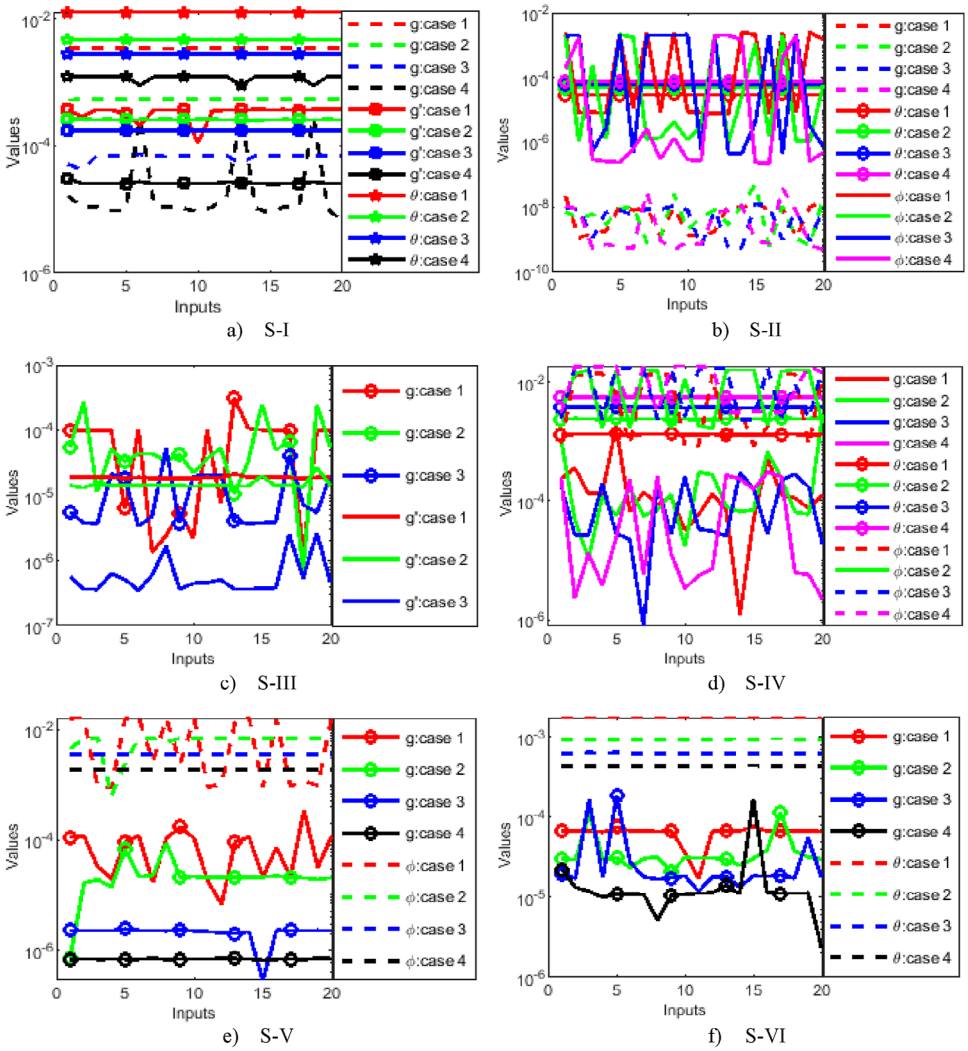

FIGURE 12 E-NSE analysis for all scenarios in MHD nanofluid flow model.

Figure 17b expresses the area graphs having an accuracy 10^{-3} to 10^{-4} using MAE in the first, second, and third cases of S-III.

5 | CONCLUSION

MHD nanofluid flow in a permeable medium over an exponentially extended surface under the heat source/sink effect is analyzed for velocity, temperature, and concentration profiles through BINNs-IMQK solver is a quite new technique. The efficacy and reliability of BINNs-IMQK solver are scrutinized by various operators. The suggested problem is solved numerically by altering the values of the A, Nb, S, R, Sc, and Pr. Unsteady parameter and suction/ injection parameter have the same effect on nanofluid velocity as both are inversely proportional to shrinking constant u_0. The parameters Nb and R have the same effect on the temperature of the suggested nanofluidic problem but this effect is overturned in the case of the Pr and A. The value of Nb has a key role in boosting the thermal conductivity of nanofluids. The Nb, R, and Sc have the same effect on the concentration of nanofluid. The proposed solver BINNs-IMQK is a remarkable alternative to solve stiff problems related to partial, fuzzy, ordinary, and fractional equations.

In future, one may exploited different combination of the global and local search methodologies along with their comparison with presented BINNs-IMQK for solving fluid mechanics problems.

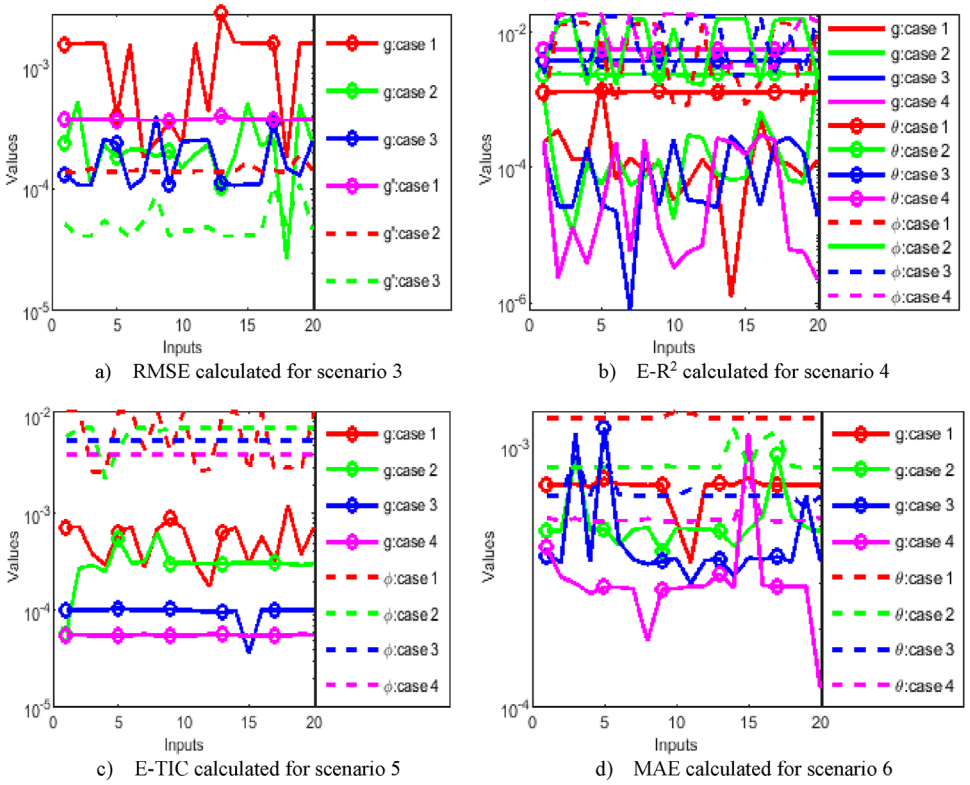

FIGURE 13 Error estimation in randomly taken scenarios using statistical operators in the suggested problem.

FIGURE 14 Fitness estimation in suggested nanofluidic problem for cases (1–3) of S-3.

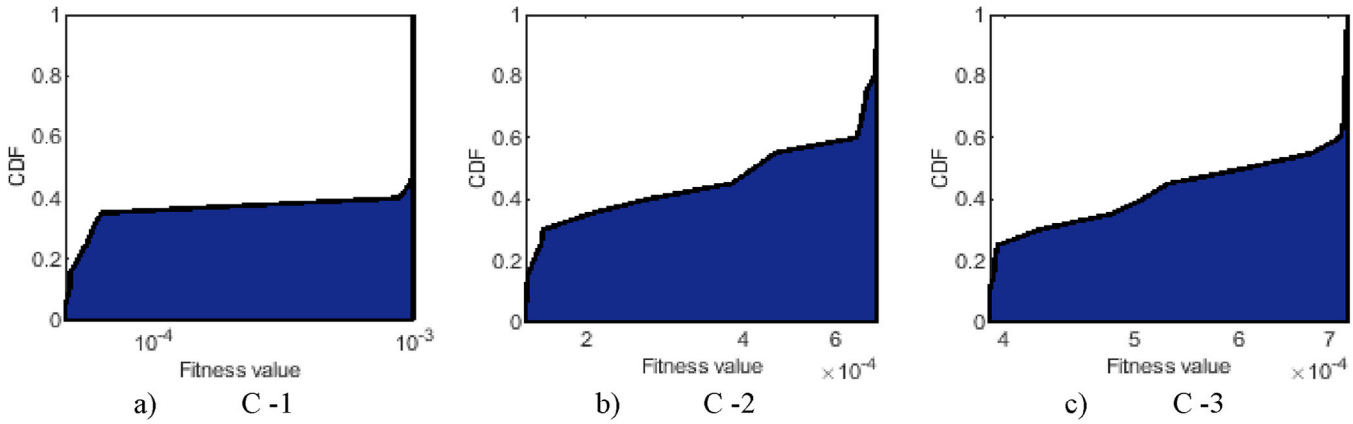

FIGURE 15 Fitness estimation through CDF in MHD nanofluid model in all three cases (for scenario 3).

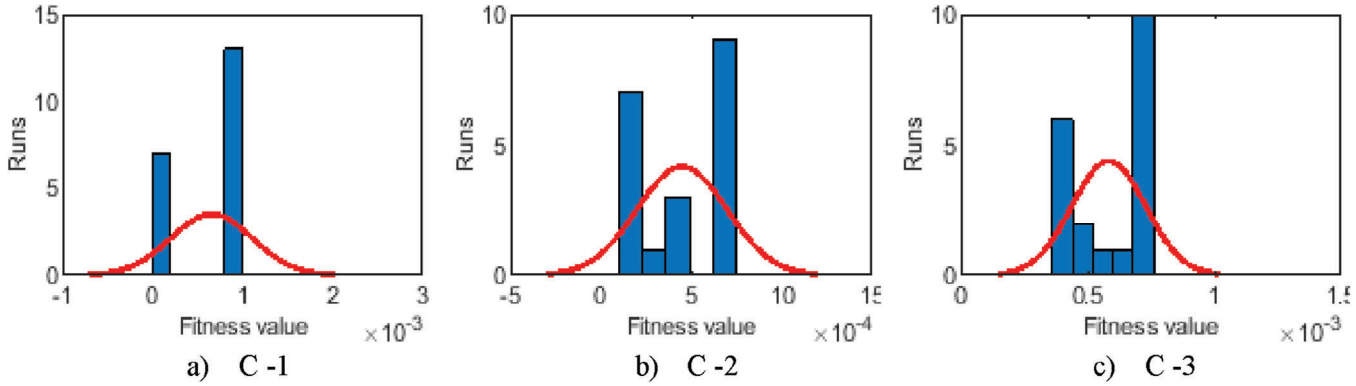

FIGURE 16 Fitness estimation through Histogram study in MHD nanofluid flow model for scenario 3.

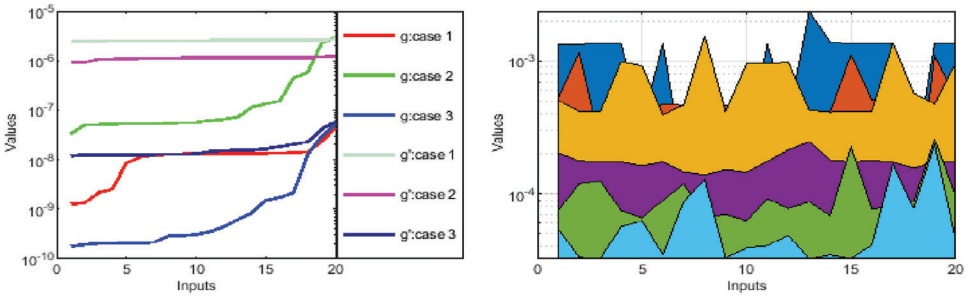

FIGURE 17 Fitness estimated through E-VAF and MAE values in MHD nanofluid flow model for scenario 3.

NOMENCLATURE

u_1, u_2	Velocity components [ms^{-1}]
Tm	Dimensional temperature [K]
B_0	Strength of magnetic field
C_p	Heat capacity [J K^{-1}]
σ	Electrical conductivity [$\Omega^{-1}m^{-1}$]
τ	Specific heat ratio [J K^{-1} kg^{-1}]
D_{Tm}	Thermophoresis diffusion coefficient
q'''	Uneven heat sink/source
M	Magnetic field parameter
L	Characteristic length
A	Unsteady parameter
Sc	Schmidt number
α_1	Diffusivity coefficient
ρ	Density of nanofluid [kg m^{-3}]
Pr	Prandtl Number
k	Thermal conductivity [Wm^{-1} K^{-1}]
Tm_∞	Ambient temperature
C_∞	Ambient level concentration [mol m^{-3}]
D_B	Brownian diffusion coefficient
C	Nanofluid dimensional concentration
W	Condition on wall/sheet
S	Suction/Injection parameter
Y	Kinematic viscosity [m^2/s]
A_1, B_1	Heat sink/source parameters

Nt Parameter for thermophoresis
N_b Brownian motion parameter
α_{Tm} Thermal diffusivity [m^2/s]
R Radiation parameter

ACKNOWLEDGMENTS

The authors have nothing to report.

CONFLICT OF INTEREST STATEMENT

The authors declare no conflicts of interest..

ORCID

Zeeshan Ikram Butt https://orcid.org/0000-0002-1793-5166
Syed Ibrar Hussain https://orcid.org/0000-0002-9391-3858
Muhammad Asif Zahoor Raja https://orcid.org/0000-0001-9953-822X

REFERENCES

[1] Choi, S.U., Eastman, J.A.: Enhancing thermal conductivity of fluids with nanoparticles (No. ANL/MSD/CP-84938; CONF-951135-29). Argonne National Lab, IL (United States) (1995)
[2] Henein, S.M., Abdel-Rehim, A.A.: The performance response of a heat pipe evacuated tube solar collector using MgO/MWCNT hybrid nanofluid as a working fluid. Case Stud. Therm. Eng. 33, 101957 (2022)
[3] Janocha, M., Tsotsas, E.: Coating layer formation from deposited droplets: A comparison of nanofluid, microfluid and solution. Powder Technol. 399, 117202 (2022)
[4] Du, R., Jiang, D., Wang, Y., Shah, K.W.: An experimental investigation of CuO/water nanofluid heat transfer in geothermal heat exchanger. Energy Build. 227, 110402 (2020)
[5] Contreras, E.M.C., Bandarra Filho, E.P.: Heat transfer performance of an automotive radiator with MWCNT nanofluid cooling in a high operating temperature range. Appl. Therm. Eng. 207, 118149 (2022)
[6] Saleem, N., Ashraf, T., Daqqa, I., Munawar, S., Idrees, N., Afzal, F., Afzal, D.: Thermal case study of cilia actuated transport of radiated blood-based ternary nanofluid under the action of tilted magnetic field. Coatings. 12(6), 873 (2022)
[7] Enjavi, Y., Sedghamiz, M.A., Rahimpour, M.R.: Application of nanofluids in drug delivery and disease treatment. In: Nanofluids and Mass Transfer, pp. 449–465. Elsevier, Dutch (Netherlands), (2022)
[8] Khiabani, N.P., Fakhroueian, Z., Bahramian, A., Vatanparast, H.: Crystal growth of magnesium oxide nanocompounds for wetting alteration of carbonate surfaces. Chem. Pap. 73(10), 2513–2524 (2019)
[9] Zhu, B., Sun, Y., Guo, P., Liu, J.: Nano-sized copper oxide enhancing the combustion of aluminum/kerosene-based nanofluid fuel droplets. Combust. Flame. 240, 112028 (2022)
[10] Gupta, M., Singh, V., Kumar, R., Said, Z.: A review on thermophysical properties of nanofluids and heat transfer applications. Renew. Sustain. Energy Rev. 74, 638–670 (2017)
[11] Jeevanandam, J., Barhoum, A., Chan, Y.S., Dufresne, A., Danquah, M.K.: Review on nanoparticles and nanostructured materials: history, sources, toxicity and regulations. Beilstein J. Nanotechnol. 9(1), 1050–1074 (2018)
[12] Ghani, S.N.A., Ul-Haq, R., Noor, N.F.M.: Engine oil enhanced performance with hybrid graphene-SWCNT nanomaterials over a Riga curvy surface. Case Stud. Therm. Eng. 45, 102902 (2023)
[13] Khan Usafzai, W., Haq, R.U., Aly, E.H.: Wall laminar nanofluid jet flow and heat transfer. Int. J. Numer. Methods Heat Fluid Flow. 33(5), 1818–1836 (2023)
[14] Haq, R.U., Sajjad, T., Usman, M., Naseem, A.: Oblique stagnation point flow of micropolar nanofluid impinge along a vertical surface via modified Chebyshev collocation method. Phys. Fluids. 34(10) (2022)
[15] Soomro, F.A., Usman, M., El-Sapa, S., Hamid, M., Haq, R.U.: Numerical study of heat transfer performance of MHD Al2O3-Cu/water hybrid nanofluid flow over inclined surface. Arch Appl. Mech. 92(9), 2757–2765 (2022)
[16] Alizadeh, M., Haq, R.U., Hamid, M., Nguyen, V.B., Truong, T.H., Ganji, D.D., Tian, Z.F.: An analysis of latent heat thermal energy storage in a hexagonal triplex-tube unit with curve shape fin and CNTs. Case Stud. Therm. Eng. 36, 102241 (2022)
[17] Ullah, M.Z., Hussain, S.T., Haq, R.U., Alzahrani, A.K., Mallawi, F.: Thermal energy performance due to convection process of nanofluid in a porous medium due to split lid motion in a right triangular enclosure. J. Comput. Des. Eng. 9(3), 890–906 (2022)
[18] Shah, S.S., ul Haq, R., McCash, L.B., Bahaidarah, H.M., Aziz, T.: Numerical simulation of lid driven flow in a curved corrugated porous cavity filled with CuO-water in the presence of heat generation/absorption. Alexandria Eng. J. 61(4), 2749–2767 (2022)
[19] Nguyen, M.N., Shah, S.S., Haq, R.U., Le, T.H., McCash, L.B.: Thermal performance of water driven flow of nanoparticle's shape due to double sided forced convection enclosed in a porous corrugated duct. J. Mol. Liq. 347, 118046 (2022)
[20] Williams, H.M.: The application of magnetic nanoparticles in the treatment and monitoring of cancer and infectious diseases. Biosci. Horiz. 10, 1–10 (2017)

[21] Abbas, W., Magdy, M.M.: Heat and mass transfer analysis of nanofluid flow based on, and over a moving rotating plate and impact of various nanoparticle shapes. Math. Probl. Eng. 2020, 1–12 (2020)
[22] Raza, J., Mebarek-Oudina, F., Ram, P., Sharma, S.: MHD flow of non-Newtonian molybdenum disulfide nanofluid in a converging/diverging channel with Rosseland radiation. In: Defect and Diffusion Forum, vol. 401, pp. 92–106. Trans Tech Publications Ltd, Switzerland (2020)
[23] Tlili, I., Ramzan, M., Kadry, S., Kim, H.W., Nam, Y.: Radiative MHD nanofluid flow over a moving thin needle with entropy generation in a porous medium with dust particles and Hall current. Entropy. 22(3), 354 (2020)
[24] Shah, Z., McCash, L.B., Dawar, A., Bonyah, E.: Entropy optimization in Darcy–Forchheimer MHD flow of water based copper and silver nanofluids with Joule heating and viscous dissipation effects. AIP Adv. 10(6), 065137 (2020)
[25] Hayat, T., Riaz, R., Aziz, A., Alsaedi, A.: Influence of Arrhenius activation energy in MHD flow of third grade nanofluid over a nonlinear stretching surface with convective heat and mass conditions. Physica A. 549, 124006 (2020)
[26] Sobamowo, M.G., Yinusa, A.A., Akinshilo, A.T.: Homotopy analysis method to MHD-slip flow of an upper-convected maxwell viscoelastic nanofluid in a permeable channel embedded in a porous medium. Int. J. Petrochem. Sci. Eng. 5, 11–20 (2020)
[27] Gupta, S., Kumar, D., Singh, J.: Analytical study for MHD flow of Williamson nanofluid with the effects of variable thickness, nonlinear thermal radiation and improved Fourier's and Fick's Laws. SN Appl. Sci. 2(3), 1–12 (2020)
[28] Alreshidi, N.A., Shah, Z., Dawar, A., Kumam, P., Shutaywi, M., Watthayu, W.: Brownian motion and thermophoresis effects on MHD three dimensional nanofluid flow with slip conditions and Joule dissipation due to porous rotating disk. Molecules. 25(3), 729 (2020)
[29] Raghunath, K., Obulesu, M., Sivaprasad, R.: Heat and mass transfer on an unsteady MHD flow through porous medium between two porous vertical plates. In: *AIP Conference Proceedings*, Vol. 2220, No. 1, p. 130003. AIP Publishing LLC, USA (2020)
[30] Sreedevi, P., Sudarsana Reddy, P., Sheremet, M.A.: Impact of homogeneous–heterogeneous reactions on heat and mass transfer flow of Au–Eg and Ag–Eg Maxwell nanofluid past a horizontal stretched cylinder. J. Therm. Anal. Calorim. 141(1), 533–546 (2020)
[31] Gireesha, B.J., Kumar, K.G., Ramesh, G.K., Prasannakumara, B.C.: Nonlinear convective heat and mass transfer of Oldroyd-B nanofluid over a stretching sheet in the presence of uniform heat source/sink. Results Phys. 9, 1555–1563 (2018)
[32] Rizwan, A., Ahmad, I., Raja, M.A.Z., Shoaib, M.: Design of spline–evolutionary computing paradigm for nonlinear thin film flow model. Arab J. Sci. Eng. 46(9), 9279–9299 (2021)
[33] Ali, S., Ahmad, I., Raja, M.A.Z., Ahmad, S.U.I., Shoaib, M.: Design of evolutionary cubic spline intelligent solver for nonlinear Painlevé-I transcendent. Int. J. Mod. Phys. B. 35(29), 2150299 (2021)
[34] Khan, I., Raja, M.A.Z., Khan, M.A.R., Shoaib, M., Islam, S., Shah, Z.: Design of backpropagated intelligent networks for nonlinear second-order Lane–Emden pantograph delay differential systems. Arab J. Sci. Eng. 47(2), 1197–1210 (2022)
[35] Faieq, A.K., Mijwil, M.M.: Prediction of heart diseases utilising support vector machine and artificial neural network. Indones. J. Electr. Eng. Comput. Sci. 26(1), 374–380 (2022)
[36] Shoaib, M., Raja, M.A.Z., Farhat, I., Shah, Z., Kumam, P., Islam, S.: Soft computing paradigm for Ferrofluid by exponentially stretched surface in the presence of magnetic dipole and heat transfer. Alexandria Eng. J. 61(2), 1607–1623 (2022)
[37] Khan, W.U., Raja, M.A.Z., He, Y., Chaudhary, N.I.: A novel application of integrated grasshopper optimization heuristics for attenuation of noise interferences. Ain Shams Eng. J. 13(2), 101536 (2022)
[38] Ilyas, H., Raja, M.A.Z., Ahmad, I., Shoaib, M.: A novel design of Gaussian wavelet neural networks for nonlinear Falkner-Skan systems in fluid dynamics. Chin. J. Phys. 72, 386–402 (2021)
[39] Zhang, Y., Lin, J., Hu, Z., Khan, N.A., Sulaiman, M.: Analysis of third-order nonlinear multi-singular Emden–Fowler equation by using the LeNN-WOA-NM algorithm. IEEE Access. 9, 72111–72138 (2021)
[40] Umar, M., Kusen Raja, M.A.Z., Sabir, Z., Al-Mdallal, Q.: A computational framework to solve the nonlinear dengue fever SIR system. Comput. Meth. Biomech. Biomed. Eng. 25(16), 1–14 (2022)
[41] Khan, A.A., Shah, S.M., Raja, M.A.Z., Chaudhary, N.I., He, Y., Machado, J.A.: Fractional LMS and NLMS algorithms for line echo cancellation. Arab J. Sci. Eng. 46(10), 9385–9398 (2021)
[42] Muhammad, Y., Akhtar, R., Khan, R., Ullah, F., Raja, M.A.Z., Machado, J.A.: Design of fractional evolutionary processing for reactive power planning with FACTS devices. Sci. Rep. 11(1), 1–29 (2021)
[43] Shoaib, M., Raja, M.A.Z., Sabir, M.T., Bukhari, A.H., Alrabaiah, H., Shah, Z., Kumam, P., Islam, S.: A stochastic numerical analysis based on hybrid NAR-RBFs networks nonlinear SITR model for novel COVID-19 dynamics. Comput. Methods Programs Biomed. 202, 105973 (2021)
[44] Faisal, F., Shoaib, M., Raja, M.A.Z.: A new heuristic computational solver for nonlinear singular Thomas–Fermi system using evolutionary optimized cubic splines. Eur. Phys. J C Part Fields. 135(1), 55 (2020)
[45] Zameer, A., Arshad, J., Khan, A., Raja, M.A.Z.: Intelligent and robust prediction of short term wind power using genetic programming based ensemble of neural networks. Energy Convers. Manage. 134, 361–372 (2017)
[46] Ahmad, I., Raja, M.A.Z., Ramos, H., Bilal, M., Shoaib, M.: Integrated neuro-evolution-based computing solver for dynamics of nonlinear corneal shape model numerically. Neural. Comput. Appl. 33(11), 5753–5769 (2021)
[47] Chaudhary, N.I., Raja, M.A.Z., He, Y., Khan, Z.A., Machado, J.T.: Design of multi innovation fractional LMS algorithm for parameter estimation of input nonlinear control autoregressive systems. Appl. Math. Modell. 93, 412–425 (2021)
[48] Ilyas, H., Ahmad, I., Raja, M.A.Z., Tahir, M.B., Shoaib, M.: Neuro-intelligent mappings of hybrid hydro-nanofluid Al2O3–Cu–H2O model in porous medium over rotating disk with viscous dissolution and Joule heating. Int. J. Hydrogen Energy. 46(55), 28298–28326 (2021)

[49] Kumar, G.V., Rehman, K.U., Kumar, R.V.M.S.S.K., Shatanawi, W.: Unsteady magnetohydrodynamic nanofluid flow over a permeable exponentially surface manifested with non-uniform heat source/sink effects. Waves Random Complex Media. 1–19 (2022)
[50] Bhattacharyya, K., Pop, I.: MHD boundary layer flow due to an exponentially shrinking sheet. Magnetohydrodynamics. 47(4), 337–344 (2011)
[51] Franke, R.: Scattered data interpolation: tests of some methods. Math. Comput. 38(157), 181–200 (1982)
[52] Butt, Z.I., Ahmad, I., Shoaib, M., Ilyas, H., Kiani, A.K., Raja, M.A.Z.: Neuro-evolution heuristics for Prandtl-Eyring nanofluid flow with homogenous/heterogeneous reaction across a linearly heated stretched sheet. Waves Random Complex Media. 1–47 (2023). https://doi.org/10.1080/17455030.2022.2155325
[53] Butt, Z.I., Ahmad, I., Ilyas, H., Shoaib, M., Raja, M.A.Z.: Design of inverse multiquadric radial basis neural networks for the dynamical analysis of MHD casson nanofluid flow along a nonlinear stretchable porous surface with multiple slip conditions. Int. J. Hydrogen Energy 48, 16100–16131 (2023). https://doi.org/10.1016/j.ijhydene.2022.12.319
[54] Li, R., Xu, A., Zhao, Y., Chang, H., Li, X., Lin, G.: Genetic algorithm (GA)-Artificial neural network (ANN) modeling for the emission rates of toxic volatile organic compounds (VOCs) emitted from landfill working surface. J. Environ. Manage. 305, 114433 (2022)
[55] Singh, V.K., Panda, K.C., Sagar, A., Al-Ansari, N., Duan, H.F., Paramaguru, P.K., Vishwakarma, D.K., Kumar, A., Kumar, D., Kashyap, P.S., Singh, R.M.: Novel Genetic Algorithm (GA) based hybrid machine learning-pedotransfer Function (ML-PTF) for prediction of spatial pattern of saturated hydraulic conductivity. Eng. Appl. Comput. Fluid Mech. 16(1), 1082–1099 (2022)
[56] Butt, Z.I., Ahmad, I., Shoaib, M., Ilyas, H., Raja, M.A.Z.: A novel design of inverse multiquadric radial basis neural networks to analyze MHD nanofluid boundary layer flow past a wedge embedded in a porous medium under the influence of radiation and viscous effects. Int. Commun. Heat Mass Transfer. 140, 106516 (2023)
[57] Shoaib, M., Tabassum, R., Raja, M.A.Z., Nisar, K.S., Alqahtani, M.S., Abbas, M.: A design of predictive computational network for transmission model of Lassa fever in Nigeria. Results Phys. 39, 105713 (2022)
[58] Butt, Z.I., Ahmad, I., Shoaib, M.: Design of inverse multiquadric radial basis neural networks for the dynamical analysis of wire coating problem with Oldroyd 8-constant fluid. AIP Adv. 12(10), 105306 (2022)
[59] Butt, Z.I., Ahmad, I., Shoaib, M., Ilyas, H., Raja, M.A.Z.: Electro-magnetohydrodynamic impact on Darrcy-Forchheimer viscous fluid flow over a stretchable surface: Integrated intelligent Neuro-evolutionary computing approach. Int. Commun. Heat Mass Transfer. 137, 106262 (2022)

How to cite this article: Butt, Z.I., Ahmad, I., Hussain, S.I., Raja, M.A.Z., Shoaib, M., Ilyas, H.: Inverse multiquadric kernel-based neuro heuristic approach to analyze the unsteady MHD nanofluid flow via permeable elongating surface. Z Angew Math Mech. 104, e202300390 (2024). https://doi.org/10.1002/zamm.202300390